





RESEARCH ARTICLE | MAY 12 2021

Interaction of ocean wave with a harbor covered by an ice sheet

Z. F. Li (李志富) ; Y. Y. Shi (石玉云) ; G. X. Wu (吴国雄)  



Physics of Fluids 33, 057109 (2021)

<https://doi.org/10.1063/5.0051376>



Physics of Fluids

Special Topic:

John Michael Dealy (1937-2024): Celebrating His Life

Guest Editors: Alan Jeffrey Giacomini and Savvas G. Hatzikiriakos

[Submit Today!](#)

Interaction of ocean wave with a harbor covered by an ice sheet

Cite as: Phys. Fluids **33**, 057109 (2021); doi: [10.1063/5.0051376](https://doi.org/10.1063/5.0051376)

Submitted: 25 March 2021 · Accepted: 22 April 2021 ·

Published Online: 12 May 2021






View Online



Export Citation



CrossMark

Z. F. Li (李志富),¹  Y. Y. Shi (石玉云),¹  and G. X. Wu (吴国雄)^{2,a)} 

AFFILIATIONS

¹School of Naval Architecture and Ocean Engineering, Jiangsu University of Science and Technology, Zhenjiang 212003, China

²Department of Mechanical Engineering, University College London, Torrington Place, London WC1E 7JE, United Kingdom

^{a)}Author to whom corresponding should be addressed: g.wu@ucl.ac.uk

ABSTRACT

A domain decomposition method is developed to solve the problem of wave motion inside a harbor with its surface covered by an ice sheet. The shape of the horizontal plane of the harbor can be arbitrary while the sidewall is vertical. The entrance of the harbor is open to the sea with a free surface. The linearized velocity potential theory is adopted for fluid flow, and the thin elastic plate model is applied for the ice sheet. The domain is divided into two subdomains. Inside the harbor, the velocity potential is expanded into a series of eigenfunctions in the vertical direction. The orthogonal inner product is adopted to impose the impermeable condition on the harbor wall, together with the edge conditions on the intersection of the harbor wall and the ice sheet. In the open sea outside of the harbor, through the modified Green function, the velocity potential is written in terms of an integral equation over the surface of the harbor entrance, or the interface between the two subdomains. On the interface, the orthogonal inner product is also applied to impose the continuity conditions of velocity and pressure as well as the free ice edge conditions. Computations are first carried out for a rectangular harbor without the ice sheet to verify the methodology, and then extensive results and discussions are provided for a harbor of a more general shape covered by an ice sheet with different thicknesses and under different incident wave angles.

© 2021 Author(s). All article content, except where otherwise noted, is licensed under a Creative Commons Attribution (CC BY) license (<http://creativecommons.org/licenses/by/4.0/>). <https://doi.org/10.1063/5.0051376>

I. INTRODUCTION

A harbor can generally provide some protection to ships from ocean wave excitation. However, because the fluid domain is in a confined space, it may experience resonance. To understand the nature of the fluid motion inside a harbor is of important practical relevance. In general, the water surface inside the harbor is free. However, in some cold regions, the water surface may become frozen or covered by an ice sheet, while away from the harbor the water surface remains free. In such a case, the free surface wave may propagate into the harbor and create complex fluid ice sheet interaction. The present work tries to shed some light on the mechanism of such a process.

When there is no ice sheet on the water surface in the harbor, there has been extensive research on interactions of external waves with internal fluid motion. Mcnown¹ derived an analytical solution for a circular harbor with a small entrance at which the flow into the harbor was prescribed. This was later extended to a harbor with a rectangular shape by Kravtchenko and Mcnown.² However, in the real situation, the flow into the harbor is unknown. It depends on the interaction between flows inside and outside the harbor, which itself is part of the solution. Hwang and Tuck³ constructed a boundary integral

equation over the harbor and coastal walls, and the latter was truncated at a finite distance far away from the entrance for numerical computations. Lee⁴ introduced a domain decomposition method, in which the need to include the coastal wall in the integral equation was removed and there was no truncation error involved. A partial reflection boundary condition was used by Isaacson and Qu⁵ on the harbor boundary, which absorbs the wave energy similar to the effect of viscosity. Hamanaka⁶ considered a more general problem in which the harbor could contain several types of boundary, i.e., reflection boundary, partial reflection boundary, open boundary, and incident-absorbing boundary. The wave diffraction problem by a harbor was also considered by Kumar *et al*⁷ through the two-dimensional boundary integral method with Chebyshev point discretization applied on the horizontal plane of the harbor boundary, together with the vertical modes. However, when there is a body of general shape floating in the harbor, the problem needs to be considered in a three-dimensional sense, e.g., solved by Shi, Li, and Wu⁸ through introducing a domain decomposition method.

Also, there has been growing interest in the wave/ice sheet interactions, in the context of geophysics and polar engineering. In many

cases, the wave motion of the fluid can be described through the linearized velocity potential theory while the ice sheet deflection can be modeled by a thin elastic plate. This model is valid for a wide range of problems in the polar regions, as explained in the review papers by Squire.^{9,10} For wave propagation from open sea to the semi-infinite ice sheet, Fox and Squire¹¹ obtained the wave reflection and transmission coefficients through the matched eigenfunction expansions, where the conjugate gradient method was applied to impose the matching conditions at the interface and the ice edge conditions. When the wavenumber for free surface wave is larger than that for flexural-gravity wave in the ice sheet a critical angle exists for the incident wave. Similar to Snell's law, when the angle between the wave direction and the ice edge is smaller than this critical angle, there will be no progressing wave into the ice sheet.¹² The same problem was considered by Sahoo *et al.*,¹³ who obtained the unknowns through introducing an orthogonal inner product. Various ice edge conditions were considered. In addition, the problem has been solved through the Wiener-Hopf method by Evans and Davies,¹⁴ Balmforth and Craster,¹⁵ Chung and Fox¹⁶ and Tkacheva.¹⁷ In Balmforth and Craster,¹⁵ it was shown that for a wide range of thickness of the ice sheet, the Kirchhoff-Love model for a thin elastic plate would give similar results to those by the Timoshenko–Mindlin model which included the effects of rotary inertia and transverse shear force of the plate. Solutions have also been obtained through the residue calculus technique, for example, by Linton and Chung.¹⁸ For wave interaction with an ice sheet of finite length, by introducing the large length assumption, Meylan and Squire¹⁹ obtained an approximate solution for the two-dimensional problem, based on that for waves from open water to the semi-infinite ice sheet. It was found that there would be an infinite number of discrete frequencies at which perfect transmission would occur. The problem was solved without the large length assumption through the Green function method by Meylan and Squire,²⁰ which was then extended to solve wave interactions with a circular ice floe in the three-dimensional case.²¹ For ice floe with an arbitrary shape, Wang and Meylan²² developed a numerical scheme based on the boundary element method for fluid flow and finite element method for the ice sheet deflection. Based on the wide spacing assumption, Shi, Li, and Wu²³ solved the problem of wave interactions with multiple ice floes separated by wide polynyas, and the results showed a good agreement with those without the approximation. When the width of polynya tends to zero, it will become a crack. Li, Wu, and Ji²⁴ derived a Green function which itself satisfied the conditions at the crack. This enables the diffraction potential by the crack to be written explicitly. The Green function was then extended for an ice sheet with multiple cracks. For a closed circular crack, Li, Wu, and Shi²⁵ obtained a semi-analytical solution by expanding the unknowns into Fourier series along the crack, and the near-resonant wave motions were found when the wave frequency is close to the natural frequency of the inner ice sheet. Similar behavior was also observed by Li, Wu, and Ren²⁶ for mixed open and closed cracks. Brocklehurst *et al.*²⁷ derived an analytical solution for flexural-gravity wave reflection by a vertical wall in the two-dimensional case, in which the ice sheet extended to infinity at one end and clamped to the wall at the other end. Instead of using the integral transform method, Bhattacharjee and Soares²⁸ solved the same problem through the matched eigenfunction expansions. For three-dimensional problems, Brocklehurst *et al.*²⁹ investigated flexural-gravity wave diffraction by a vertical wall of circular cross

section. The ice sheet was of infinite extent, and the results were obtained through a Weber transform. Recently, Korobkin *et al.*³⁰ reconsidered the problem through a vertical mode method, while Ren *et al.*³¹ extended the problem to multiple vertical circular walls.

The previous work on wave motion in the harbor is for a harbor with open free surface, while the work on the ice sheet is for the surface of infinite or semi-infinite extent. Here, we shall consider the problem of the wave from the sea propagating into a frozen harbor, and its excited fluid motion inside the harbor as well as the ice sheet deflection. The harbor has vertical wall boundary and constant depth while its horizontal plane has an arbitrary shape. As external water surface is free and internal water surface is covered by an ice sheet, an efficient approach is to use the domain decomposition method. The total fluid domain is divided into two subregions, i.e., one region inside the harbor and the other region outside the harbor. In the former, the velocity potential is expanded into a series of eigenfunctions in the vertical direction, which satisfies the ice sheet condition analytically. To impose the boundary conditions on the vertical harbor wall and the edge of ice sheet, an orthogonal inner product is applied. In the region outside the harbor, a boundary integral equation is established over the interface of the two subregions and the part over the coastal line is removed analytically. On the interface, the continuities of both pressure and velocity are satisfied through the orthogonal inner product.

The paper is organized as follows. The mathematical problem for wave interaction with a frozen harbor of arbitrary geometry is formulated in Sec. II. The solution method is constructed in Sec. III, i.e., a series of eigenfunction expansions in the vertical direction in the interior region in Sec. III A, a boundary integral equation over the interface in the exterior region in Sec. III B, matching procedure through an orthogonal inner product in Sec. III C, and numerical discretization through boundary element method in Sec. III D. In Sec. IV, verifications of the proposed method are first carried out, and then a case study for a given harbor shape is provided. Conclusions are drawn in Sec. V.

II. MATHEMATICAL MODEL

The problem of wave interaction with a frozen harbor bounded by vertical walls and with arbitrary shape in the horizontal plane is sketched in Fig. 1. The region inside the harbor is covered by an ice sheet, while the region outside the harbor is fully free. The water depth H is assumed to be constant. To describe the problem, a Cartesian coordinate system $O - xyz$ is defined, with $O - xy$ plane being the undisturbed mean free water surface, and z axis pointing vertically upwards. The entrance of the harbor is in the $O - yz$ plane, and the coastal wall is along the y axis and assumed to extend to infinity. The edge of the ice sheet or its intersection with the harbor can be described parametrically by

$$\Gamma = (x(s), y(s))(-\gamma < s < +\gamma), \quad (1)$$

where 2γ is the total arc length of the edge, and s is the curvilinear coordinate along the edge. To develop the numerical procedure, the total fluid domain Ω is divided into two subregions, i.e., Ω_1 inside the harbor and Ω_2 outside the harbor, as shown in the figure.

The fluid of density ρ_w is assumed to be inviscid, incompressible, and homogeneous, and its motion to be irrotational. Thus, the velocity potential Φ can be introduced to describe the fluid flow. When the amplitude of wave motion is small compared with its length, the

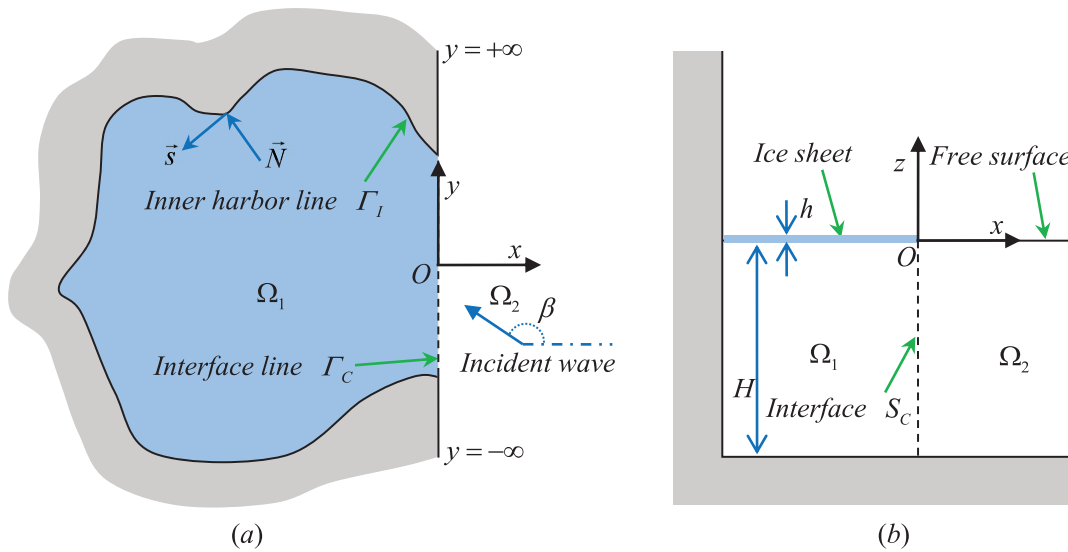


FIG. 1. Coordinate system and sketch of the problem. (a) Plane view with $z = 0$; (b) view for cross section along $O - xz$ plane with $y = 0$.

linearization of boundary conditions can be further adopted. For sinusoidal motion in time with radian frequency ω , the total velocity potential can be written as

$$\Phi^{(j)}(x, y, z, t) = \text{Re} \left\{ i\omega\eta \left[\delta_{2,j}\phi_I(x, y, z) + \phi^{(j)}(x, y, z) \right] e^{i\omega t} \right\} \quad (j = 1, 2), \quad (2)$$

where $\delta_{i,j}$ is the Kronecker delta function, ϕ_I is the incident velocity potential, and η is the complex amplitude of the incident wave. The superscripts $j = 1$ and $j = 2$ correspond to the velocity potential in the interior and exterior subregions, respectively. The conservation of mass requires that the velocity potential $\phi^{(j)}$ should satisfy the Laplace equation,

$$\nabla^2 \phi^{(j)} + \frac{\partial^2 \phi^{(j)}}{\partial z^2} = 0, \quad (3)$$

throughout the fluid, where

$$\nabla^2 = \frac{\partial^2}{\partial x^2} + \frac{\partial^2}{\partial y^2}, \quad (4)$$

is the Laplacian in the horizontal plane. Following Squire³² and others, the ice sheet inside the harbor can be modeled as a thin elastic plate with its draught effect being ignored. By assuming that the ice sheet is in contact with the fluid at all points for all time, the displacement and pressure on their interface should be continuous. The kinematic condition on the ice sheet can be written as

$$\frac{\partial W}{\partial t} = \frac{\partial \Phi^{(1)}}{\partial z} \quad (z = 0). \quad (5)$$

The deflection of the ice sheet is governed by³³

$$L\nabla^4 W + m \frac{\partial^2 W}{\partial t^2} = -\rho_w \left(\frac{\partial \Phi^{(1)}}{\partial t} + gW \right) \quad (z = 0), \quad (6)$$

where g is the acceleration due to gravity, $L = Eh^3/[12(1 - \nu^2)]$ and $m = \rho_i h$ are, respectively, the effective flexural rigidity and mass per unit area of the ice sheet, with its Young's modulus E , Poisson's ratio ν , density ρ_i , and thickness h being assumed to be constant. The right hand side of Eq. (6) is in fact the fluid pressure. Similar to the velocity potential in Eq. (2), we may write the deflection of the ice sheet as

$$W(x, y, t) = \text{Re} \left[\eta w(x, y) e^{i\omega t} \right]. \quad (7)$$

Combining Eqs. (5) and (6), and using (2) and (7), the boundary condition for the velocity potential on the ice sheet can be written as

$$(L\nabla^4 + \rho_w g - m\omega^2) \frac{\partial \phi^{(1)}}{\partial z} - \rho_w \omega^2 \phi^{(1)} = 0 \quad (z = 0). \quad (8)$$

Without loss of generality, the edge of the ice sheet inside the harbor is assumed to be clamped to the vertical wall, which means that both the displacement and the slope there are zero, i.e.,

$$w = 0 \quad \text{and} \quad \frac{\partial w}{\partial N} = 0 \quad ((x, y) \in \Gamma_I, z = 0), \quad (9)$$

or

$$\frac{\partial \phi^{(1)}}{\partial z} = 0 \quad \text{and} \quad \frac{\partial^2 \phi^{(1)}}{\partial N \partial z} = 0 \quad ((x, y) \in \Gamma_I, z = 0), \quad (10)$$

where $\vec{N} = (\cos \Theta, \sin \Theta)$ is the unit vector along the normal direction of Γ_I or the harbor wall as shown in Fig. 1. On the vertical wall of the harbor, the impermeable condition should be satisfied which states that

$$\frac{\partial \phi^{(1)}}{\partial N} = 0 \quad ((x, y) \in \Gamma_I, z \in [-H, 0]). \quad (11)$$

The ice edge at the interface of the two subregions Ω_1 and Ω_2 is free of bending moment and shear force, i.e.,³³

$$\mathcal{B}\left(\frac{\partial\phi^{(1)}}{\partial z}\right) = 0 \quad \text{and} \quad \mathcal{S}\left(\frac{\partial\phi^{(1)}}{\partial z}\right) = 0 \quad ((x, y) \in \Gamma_C, z = 0), \quad (12)$$

where the operators \mathcal{B} and \mathcal{S} are, respectively, defined as

$$\mathcal{B} = \nabla^2 - \nu_0 \left(\sin^2\Theta \frac{\partial^2}{\partial x^2} + \cos^2\Theta \frac{\partial^2}{\partial y^2} - \sin 2\Theta \frac{\partial^2}{\partial x \partial y} \right), \quad (13)$$

$$\mathcal{S} = \frac{\partial}{\partial n} \nabla^2 + \nu_0 \frac{\partial}{\partial s} \left[\cos 2\Theta \frac{\partial^2}{\partial x \partial y} + \frac{\sin 2\Theta}{2} \left(\frac{\partial^2}{\partial y^2} - \frac{\partial^2}{\partial x^2} \right) \right], \quad (14)$$

with $\nu_0 = 1 - \nu$, and $\vec{N} = (\cos \Theta, \sin \Theta)$ and $\vec{s} = (-\sin \Theta, \cos \Theta)$ are the unit vectors along the normal and tangential directions of Γ_C , respectively. In the subregion outside the harbor, the combination of linearized dynamic and kinematic free surface boundary conditions yields

$$-\omega^2 \phi^{(2)} + g \frac{\partial \phi^{(2)}}{\partial z} = 0 \quad (z = 0). \quad (15)$$

At infinity the radiation condition requires that the diffracted waves should propagate outwards, or

$$\lim_{r_h \rightarrow \infty} \sqrt{r_h} \left(\frac{\partial \phi^{(2)}}{\partial r_h} + ik_0 \phi^{(2)} \right) = 0, \quad (16)$$

where $r_h^2 = x^2 + y^2$, $i = \sqrt{-1}$, and k_0 is the wavenumber and is the purely positive real root of the dispersion equation for the gravity wave in the open sea,

$$K_2(\omega, k) \equiv gk \tanh(kH) - \omega^2 = 0. \quad (17)$$

On the flat seabed, we have

$$\frac{\partial \phi^{(j)}}{\partial z} = 0 \quad (j = 1, 2, z = -H). \quad (18)$$

III. SOLUTION PROCEDURES

As can be seen from the above section, the boundary condition for the velocity potential on the upper surface is nonuniform. Inside the harbor Ω_1 , the ice sheet boundary condition (8) should be satisfied together with the ice edge conditions (10) and (12) along Γ_I and Γ_C , respectively. While outside the harbor Ω_2 which extends from the straight coastline to infinity, free surface boundary condition (15) should be enforced. Although the subregion Ω_1 is finite, the condition on the ice sheet contains high derivative up to the fifth order, which is usually a major challenge in numerical calculation. An effective way to solve such a problem with nonuniform upper surface boundary condition is to use a different method in each subregion, and then match the solutions in the two subregions on their interface.

A. Series expansion in the interior region Ω_1 of the harbor

In the ice covered region Ω_1 inside the harbor, through applying the variable separation method, we have³⁴

$$\phi^{(1)}(p) = \sum_{m=-2}^{\infty} \varphi_m(x, y) \psi_m(z), \quad (19)$$

where

$$\nabla^2 \varphi_m + \kappa_m^2 \varphi_m = 0, \quad (20)$$

and

$$\psi_m(z) = \frac{\cosh[\kappa_m(z+h)]}{\cosh(\kappa_m h)}, \quad (21)$$

with κ_m being the roots of the dispersion equation for ice sheet or

$$K_1(\omega, \kappa) \equiv (L\kappa^4 + \rho_w g - m\omega^2) \kappa \tanh(\kappa h) - \rho_w \omega^2 = 0. \quad (22)$$

It may be noticed that κ_{-2} and κ_{-1} are two complex roots with negative imaginary parts and symmetric about the imaginary axis, κ_0 is the purely positive real root, κ_m ($m = 1, 2, \dots$) are an infinite number of purely negative imaginary roots. To convert the two dimensional Helmholtz equation in Eq. (20) into an integral equation over $\Gamma = \Gamma_I + \Gamma_C$, we may use the Green function,³⁵

$$G^{(1)}(p, q) = \frac{\pi}{2i} H_0^{(2)}(\kappa_m R), \quad (23)$$

where $H_0^{(2)}(\kappa_m R)$ is the zero order Hankel function of second kind,³⁶ and R is the horizontal distance between the field point $p(x, y, z)$ and the source point $q(\xi, \eta, \zeta)$. Applying Green's identity to $G^{(1)}(p, q)$ and φ_m , we have

$$\alpha^{(1)}(p) \varphi_m(p) = \int_{\Gamma} \left[G^{(1)}(p, q) \frac{\partial \varphi_m(q)}{\partial N} - \frac{\partial G^{(1)}(p, q)}{\partial N} \varphi_m(q) \right] dl, \quad (24)$$

where $\alpha^{(1)}$ is the two-dimensional solid angle at field point p .

To impose the impermeable condition on the vertical harbor wall, we may use the following inner product,¹³

$$\langle \psi_m, \psi_{\tilde{m}} \rangle = \int_{-H}^0 \psi_m \psi_{\tilde{m}} dz + \frac{L}{\rho_w \omega^2} \left(\frac{d\psi_m}{dz} \frac{d^3 \psi_{\tilde{m}}}{dz^3} + \frac{d^3 \psi_m}{dz^3} \frac{d\psi_{\tilde{m}}}{dz} \right)_{z=0}. \quad (25)$$

Then if $m \neq \tilde{m}$, $\langle \psi_m, \psi_{\tilde{m}} \rangle = 0$, and if $m = \tilde{m}$, $\langle \psi_m, \psi_{\tilde{m}} \rangle = Q_m$, where

$$Q_m = \frac{2\kappa_m H + \sinh(2\kappa_m H)}{4\kappa_m \cosh^2(\kappa_m H)} + \frac{2L\kappa_m^4}{\rho_w \omega^2} \tanh^2(\kappa_m H). \quad (26)$$

Applying the inner product to $\partial \phi^{(1)}/\partial n$ and $\psi_{\tilde{m}}$ on the vertical harbor wall, we have

$$\left\langle \frac{\partial \phi^{(1)}}{\partial n}, \psi_{\tilde{m}} \right\rangle = \int_{-H}^0 \frac{\partial \phi^{(1)}}{\partial n} \psi_{\tilde{m}} dz + \frac{L}{\rho_w \omega^2} \left(\frac{\partial^2 \phi^{(1)}}{\partial z \partial n} \frac{d^3 \psi_{\tilde{m}}}{dz^3} + \frac{\partial^4 \phi^{(1)}}{\partial z^3 \partial n} \frac{d\psi_{\tilde{m}}}{dz} \right)_{z=0}. \quad (27)$$

According to the boundary condition Eq. (11) on the vertical harbor wall and the clamped ice edge condition (10), both of the first and second terms on the right hand side of the above equation are zero, i.e., Eq. (27) can be rewritten as

$$\left\langle \frac{\partial \phi^{(1)}}{\partial n}, \psi_m \right\rangle = \frac{L\kappa_m \tanh(\kappa_m H)}{\rho_w \omega^2} \Upsilon, \quad (28)$$

where

$$\Upsilon = \left(\frac{\partial^4 \phi^{(1)}}{\partial z^3 \partial n} \right)_{z=0}. \tag{29}$$

Substituting Eq. (19) into (28), we have

$$\frac{\partial \varphi_m}{\partial N} = \frac{L \kappa_m \tanh(\kappa_m H)}{\rho_w \omega^2 Q_m} \Upsilon. \tag{30}$$

Here, we have used $\vec{n} = \vec{N}$ on the vertical wall. The substitution of Eqs. (30) into (24) further provides

$$\begin{aligned} & \alpha^{(1)}(p) \varphi_m(p) \\ &= \int_{\Gamma_I} \left[G^{(1)}(p, q) \frac{L \kappa_m \tanh(\kappa_m H)}{\rho_w \omega^2 Q_m} \Upsilon(q) - \frac{\partial G^{(1)}(p, q)}{\partial N} \varphi_m(q) \right] dl \\ &+ \int_{\Gamma_C} \left[G^{(1)}(p, q) \frac{\partial \varphi_m(q)}{\partial N} - \frac{\partial G^{(1)}(p, q)}{\partial N} \varphi_m(q) \right] dl. \end{aligned} \tag{31}$$

B. Boundary integral equation in the exterior region Ω_2 of the harbor

In the exterior region Ω_2 of the harbor bounded by the coastline $x = 0$, we may divide the total velocity potential $\phi^{(2)}$ into three parts or⁸

$$\phi^{(2)} = \phi_I + \phi_I^{(2)} + \phi_D^{(2)}, \tag{32}$$

where

$$\phi_I(x, y, z) = \varphi_I(x, y) Z_0(z), \tag{33}$$

$$\phi_I^{(2)}(x, y, z) = \phi_I(-x, y, z) = \bar{\varphi}_I(x, y) Z_0(z), \tag{34}$$

with $\bar{\varphi}_I(x, y) = \varphi_I(-x, y)$ and

$$\varphi_I(x, y) = \frac{g}{\omega^2} e^{-ik_0(x \cos \beta + y \sin \beta)}. \tag{35}$$

Here, $\phi_I^{(2)}$ is the diffracted potential of ϕ_I by the coastline at $x = 0$, while $\phi_D^{(2)}$ is that by the harbor, k_0 is the real solution of Eq. (17) and $Z_0(z)$ will be defined later in Eq. (54). It may be noticed that $\phi_I^{(2)}$ has been taken out separately because it does not decay as $x \rightarrow \infty$. Away from the harbor, $\phi_D^{(2)}$ will behave like a ring wave and will decay in a rate proportional to the square root of the distance to the harbor. Applying Green's identity to $G^{(2)}(p, q)$ and $\phi_D^{(2)}$, we have

$$\alpha^{(2)}(p) \phi_D^{(2)}(p) = \int_{S_C} \left[G^{(2)}(p, q) \frac{\partial \phi_D^{(2)}(q)}{\partial n} - \frac{\partial G^{(2)}(p, q)}{\partial n} \phi_D^{(2)}(q) \right] ds, \tag{36}$$

where both the derivative and integration are performed with respect to q , $\alpha^{(2)}$ is the solid angle at point p , and S_C is the interface of Ω_1 and Ω_2 . In Eq. (36), $G^{(2)} = G + \bar{G}$, where G is the free surface Green function for open water or³⁷

$$\begin{aligned} G(p, q) &= \frac{1}{r_1} + \frac{1}{r_2} + 2 \int_0^{+\infty} e^{-kH} \frac{gk + \omega^2}{gk \tanh(kH) - \omega^2} \\ &\times \frac{\cosh[k(\zeta + H)]}{\cosh(kH)} \cosh[k(z + H)] J_0(kR) dk, \end{aligned} \tag{37}$$

with $\bar{G} = G(p, \bar{q})$ and $\bar{q}(-\xi, \eta, \zeta)$ being the mirror image of q about the coastline. The integral route in Eq. (37) from 0 to $+\infty$ should pass over the pole at $k = k_0$, r_1 is the distance between p and q , r_2 is the distance between p and the mirror image of q about the flat seabed, and $J_0(kR)$ is the zeroth-order Bessel function of first kind.³⁶

C. Matching on the interface S_C of the two subregions

On the interface S_C of the two subregions, the continuity conditions of pressure and velocity yield

$$\phi^{(1)}(x, y, z) = \phi^{(2)}(x, y, z), \tag{38}$$

$$\frac{\partial \phi^{(1)}(x, y, z)}{\partial n} = \frac{\partial \phi^{(2)}(x, y, z)}{\partial n}, \tag{39}$$

where the unit normal vector \vec{n} points outward from Ω_1 . To satisfy the continuity condition of pressure in (38), we apply inner product (25) to $\phi^{(1)}$ and $\psi_{\bar{m}}$, which provides

$$\begin{aligned} \langle \phi^{(1)}, \psi_{\bar{m}} \rangle &= \int_{-H}^0 \phi^{(1)} \psi_{\bar{m}} dz + \frac{L}{\rho_w \omega^2} \left(\frac{\partial \phi^{(1)}}{\partial z} \frac{d^3 \psi_{\bar{m}}}{dz^3} + \frac{\partial^3 \phi^{(1)}}{\partial z^3} \frac{d \psi_{\bar{m}}}{dz} \right)_{z=0} \\ &= \int_{-H}^0 \phi^{(2)} \psi_{\bar{m}} dz + \frac{L}{\rho_w \omega^2} \left(\frac{\partial \phi^{(2)}}{\partial z} \frac{d^3 \psi_{\bar{m}}}{dz^3} + \frac{\partial^3 \phi^{(2)}}{\partial z^3} \frac{d \psi_{\bar{m}}}{dz} \right)_{z=0}. \end{aligned} \tag{40}$$

Similarly, we have for the continuity condition of velocity Eq. (39) or

$$\begin{aligned} & \left\langle \frac{\partial \phi^{(1)}}{\partial n}, \psi_{\bar{m}} \right\rangle \\ &= \int_{-H}^0 \frac{\partial \phi^{(1)}}{\partial n} \psi_{\bar{m}} dz + \frac{L}{\rho_w \omega^2} \left(\frac{\partial^2 \phi^{(1)}}{\partial z \partial n} \frac{d^3 \psi_{\bar{m}}}{dz^3} + \frac{\partial^4 \phi^{(1)}}{\partial z^3 \partial n} \frac{d \psi_{\bar{m}}}{dz} \right)_{z=0} \\ &= \int_{-H}^0 \frac{\partial \phi^{(2)}}{\partial n} \psi_{\bar{m}} dz + \frac{L}{\rho_w \omega^2} \left(\frac{\partial^2 \phi^{(2)}}{\partial z \partial n} \frac{d^3 \psi_{\bar{m}}}{dz^3} + \frac{\partial^4 \phi^{(2)}}{\partial z^3 \partial n} \frac{d \psi_{\bar{m}}}{dz} \right)_{z=0}. \end{aligned} \tag{41}$$

Substituting Eq. (19) for $\phi^{(1)}$ and the corresponding $\partial \phi^{(1)} / \partial n$ into the left hand sides of Eqs. (40) and (41), respectively, we have

$$\varphi_{\bar{m}} Q_{\bar{m}} = \int_{-H}^0 \phi^{(2)} \psi_{\bar{m}} dz + \frac{L}{\rho_w \omega^2} \left(\frac{\partial \phi^{(2)}}{\partial z} \frac{d^3 \psi_{\bar{m}}}{dz^3} + \frac{\partial^3 \phi^{(2)}}{\partial z^3} \frac{d \psi_{\bar{m}}}{dz} \right)_{z=0}, \tag{42}$$

and

$$\frac{\partial \varphi_{\bar{m}}}{\partial N} Q_{\bar{m}} = \int_{-H}^0 \frac{\partial \phi^{(2)}}{\partial n} \psi_{\bar{m}} dz + \frac{L}{\rho_w \omega^2} \left(\frac{\partial^2 \phi^{(2)}}{\partial z \partial n} \frac{d^3 \psi_{\bar{m}}}{dz^3} + \frac{\partial^4 \phi^{(2)}}{\partial z^3 \partial n} \frac{d \psi_{\bar{m}}}{dz} \right)_{z=0}. \tag{43}$$

Invoking Eq. (3) or $\partial^2 \phi^{(1)} / \partial z^2 = -\nabla^2 \phi^{(1)}$, the above two equations can be rewritten as

$$\begin{aligned} \varphi_{\bar{m}} Q_{\bar{m}} &= \int_{-H}^0 \phi^{(2)} \psi_{\bar{m}} dz + \frac{L}{\rho_w \omega^2} \left(\frac{\partial \phi^{(1)}}{\partial z} \frac{d^3 \psi_{\bar{m}}}{dz^3} \right. \\ &\left. - \nabla^2 \left(\frac{\partial \phi^{(1)}}{\partial z} \right) \frac{d \psi_{\bar{m}}}{dz} \right)_{z=0}, \end{aligned} \tag{44}$$

and

$$\frac{\partial \varphi_{\bar{m}}}{\partial N} Q_{\bar{m}} = \int_{-H}^0 \frac{\partial \phi^{(2)}}{\partial n} \psi_{\bar{m}} dz + \frac{L}{\rho_w \omega^2} \left\{ \frac{\partial^2 \phi^{(1)}}{\partial z \partial N} \frac{d^3 \psi_{\bar{m}}}{dz^3} - \left[\frac{\partial}{\partial N} \nabla^2 \left(\frac{\partial \phi^{(1)}}{\partial z} \right) \right] \frac{d\psi_{\bar{m}}}{dz} \right\}_{z=0}. \quad (45)$$

The last terms in the above two equations can be replaced according to the ice edge conditions. Using

$$\frac{\partial x}{\partial s} = -\sin \Theta \quad \text{and} \quad \frac{\partial y}{\partial s} = \cos \Theta, \quad (46)$$

on Γ_C with $\Theta = 0$, the operators \mathcal{B} and \mathcal{S} in Eqs. (13) and (14) can be written as

$$\mathcal{B} = \nabla^2 - \nu_0 \left(\frac{\partial^2}{\partial s^2} + \frac{\partial \Theta}{\partial s} \frac{\partial}{\partial N} \right) = \nabla^2 - \nu_0 \frac{\partial^2}{\partial y^2}, \quad (47)$$

$$\mathcal{S} = \frac{\partial}{\partial N} \nabla^2 + \nu_0 \frac{\partial}{\partial s} \left(\frac{\partial^2}{\partial s \partial N} - \frac{\partial \Theta}{\partial s} \frac{\partial}{\partial s} \right) = \frac{\partial}{\partial N} \nabla^2 + \nu_0 \frac{\partial^3}{\partial y^2 \partial N}. \quad (48)$$

Then the free ice edge condition in Eq. (12) provides

$$\nabla^2 \left(\frac{\partial \phi^{(1)}}{\partial z} \right) = \nu_0 \frac{\partial^2}{\partial y^2} \left(\frac{\partial \phi^{(1)}}{\partial z} \right), \quad (49)$$

$$\frac{\partial}{\partial N} \nabla^2 \left(\frac{\partial \phi^{(1)}}{\partial z} \right) = -\nu_0 \frac{\partial^3}{\partial y^2 \partial N} \left(\frac{\partial \phi^{(1)}}{\partial z} \right). \quad (50)$$

Substituting Eqs. (49) and (50) into (44) and (45) respectively, we have

$$\varphi_{\bar{m}} Q_{\bar{m}} = \int_{-H}^0 \phi^{(2)} \psi_{\bar{m}} dz + \frac{L}{\rho_w \omega^2} \left[\frac{\partial \phi^{(1)}}{\partial z} \frac{d^3 \psi_{\bar{m}}}{dz^3} - \nu_0 \frac{\partial^2}{\partial y^2} \left(\frac{\partial \phi^{(1)}}{\partial z} \right) \frac{d\psi_{\bar{m}}}{dz} \right]_{z=0} \quad (51)$$

and

$$\frac{\partial \varphi_{\bar{m}}}{\partial N} Q_{\bar{m}} = \int_{-H}^0 \frac{\partial \phi^{(2)}}{\partial n} \psi_{\bar{m}} dz + \frac{L}{\rho_w \omega^2} \left\{ \frac{\partial^2 \phi^{(1)}}{\partial z \partial N} \frac{d^3 \psi_{\bar{m}}}{dz^3} + \left[\nu_0 \frac{\partial^3}{\partial y^2 \partial N} \left(\frac{\partial \phi^{(1)}}{\partial z} \right) \right] \frac{d\psi_{\bar{m}}}{dz} \right\}_{z=0}. \quad (52)$$

On the interface S_C , which is vertically extended from the seabed to the ice edge, we may expand the potential $\phi_D^{(2)}$ as well as its normal derivative into a series of orthogonal eigenfunctions,³⁷

$$\phi_D^{(2)}(p) = \sum_{m=0}^{\infty} \phi_m(x, y) Z_m(z), \quad \frac{\partial \phi_D^{(2)}(p)}{\partial n} = \sum_{m=0}^{\infty} \frac{\partial \phi_m(x, y)}{\partial N} Z_m(z), \quad (53)$$

where

$$Z_m(z) = \frac{\cosh[k_m(z + H)]}{\cosh(k_m H)}, \quad (54)$$

with k_m being the solutions of the dispersion equation (17) for free surface. In particular, k_0 is the purely positive real root, and k_m

($m = 1, 2, \dots$) are an infinite number of purely negative imaginary root. Substituting Eqs. (53) into (32), and the obtained results together with Eq. (19) into Eq. (51), we have

$$\varphi_{\bar{m}} Q_{\bar{m}} = (\varphi_I + \bar{\varphi}_I) \mathfrak{S}_{0, \bar{m}} + \sum_{m=0}^{\infty} \phi_m \mathfrak{S}_{m, \bar{m}} + \sum_{m=-2}^{\infty} \mathfrak{R}_{m, \bar{m}} \varphi_m, \quad (55)$$

where

$$\mathfrak{R}_{m, \bar{m}} = \frac{L}{\rho_w \omega^2} \left[\frac{d\psi_m}{dz} \left(\frac{d^3 \psi_{\bar{m}}}{dz^3} - \nu_0 \frac{d\psi_{\bar{m}}}{dz} \frac{\partial^2}{\partial y^2} \right) \right]_{z=0}, \quad (56)$$

$$\mathfrak{S}_{m, \bar{m}} = \int_{-H}^0 Z_m(z) \psi_{\bar{m}}(z) dz = \frac{1}{\cosh(k_m h) \cosh(\kappa_{\bar{m}} h)} \left\{ \frac{\sinh[h(k_m - \kappa_{\bar{m}})]}{2(k_m - \kappa_{\bar{m}})} + \frac{\sinh[h(k_m + \kappa_{\bar{m}})]}{2(k_m + \kappa_{\bar{m}})} \right\}. \quad (57)$$

Similarly, we have for Eq. (52),

$$\frac{\partial \varphi_{\bar{m}}}{\partial N} Q_{\bar{m}} = \sum_{m=0}^{\infty} \frac{\partial \phi_m}{\partial N} \mathfrak{S}_{m, \bar{m}} + \sum_{m=-2}^{\infty} \mathfrak{N}_{m, \bar{m}} \varphi_m, \quad (58)$$

where

$$\mathfrak{N}_{m, \bar{m}} = \frac{L}{\rho_w \omega^2} \left[\frac{d\psi_m}{dz} \left(\frac{d^3 \psi_{\bar{m}}}{dz^3} + \nu_0 \frac{d\psi_{\bar{m}}}{dz} \frac{\partial^2}{\partial y^2} \right) \frac{\partial}{\partial N} \right]_{z=0}. \quad (59)$$

Substituting Eq. (53) and the series form of Eq. (37) or

$$G(p, q) = \sum_{m=0}^{\infty} \frac{-4\pi i k_m \cosh^2(k_m H)}{2k_m H + \sinh(2k_m H)} Z_m(z) Z_m(\zeta) H_0^{(2)}(k_m R), \quad (60)$$

into (36) and using the orthogonal property of $Z_m(z)$, we can also transform the boundary integral equation in Ω_2 over the interface into the line integral over the free ice edge Γ_C , i.e.,

$$\alpha^{(2)}(p) \phi_m(p) = \int_{\Gamma_C} \left[G_m^{(2)}(p, q) \frac{\partial \phi_m(q)}{\partial N} - \frac{\partial G_m^{(2)}(p, q)}{\partial N} \phi_m(q) \right] dl, \quad (61)$$

where

$$G_m^{(2)}(p, q) = \frac{\pi}{i} \left[H_0^{(2)}(k_m R) + H_0^{(2)}(k_m \bar{R}) \right], \quad (62)$$

with \bar{R} as the horizontal distance between p and the mirror image of q about the coastline $x = 0$.

D. Numerical discretization for the coupled equations

To solve the velocity potential $\phi^{(j)}$ numerically, the harbor line Γ_I and interface line Γ_C are discretized into N_I and N_C straight-line segments. At each segment i , the variables φ_m and ϕ_m are assumed to be constant, and the boundary conditions are imposed at the center of each segment. For infinite series (19) in Ω_1 and (53) in Ω_2 , only the first M terms are kept. Higher accuracy can be obtained by using a finer mesh and more terms kept in the infinite series. Then boundary integral equation (31) can be discretized into

$$\alpha^{(1)}(p_i)\varphi_m(p_i) = \sum_{j=1}^{N_I} \int_{\Delta_j} \left[G^{(1)}(p_i, q_j) \frac{L\kappa_m \tanh(\kappa_m H)}{\rho_w \omega^2 Q_m} \Upsilon(q_j) - \frac{\partial G^{(1)}(p_i, q_j)}{\partial N} \varphi_m(q_j) \right] dl + \sum_{j=N_I+1}^{N_I+N_C} \int_{\Delta_j} \left[G^{(1)}(p_i, q_j) \frac{\partial \varphi_m(q_j)}{\partial N} - \frac{\partial G^{(1)}(p_i, q_j)}{\partial N} \varphi_m(q_j) \right] dl, \quad (63)$$

where p_i and q_j represent the center point of element i and j , respectively. Equation (63) can be rewritten in the matrix form as

$$\begin{bmatrix} \frac{\partial G_{II}^{(1)}}{\partial N} & \frac{\partial G_{IC}^{(1)}}{\partial N} \\ \frac{\partial G_{CI}^{(1)}}{\partial N} & \frac{\partial G_{CC}^{(1)}}{\partial N} \end{bmatrix} \begin{bmatrix} \varphi_m^I \\ \varphi_m^C \end{bmatrix} = \begin{bmatrix} \tilde{G}_{II}^{(1)} & G_{IC}^{(1)} \\ \tilde{G}_{CI}^{(1)} & G_{CC}^{(1)} \end{bmatrix} \begin{bmatrix} \Upsilon \\ \frac{\partial \varphi_m^C}{\partial N} \end{bmatrix}. \quad (64)$$

where the element of submatrix in the left hand side or $\partial G^{(1)}/\partial N$ is defined as

$$\left(\frac{\partial G^{(1)}}{\partial N} \right)_{ij} = \delta_{ij} \alpha^{(1)}(p_i) + \int_{\Delta_j} \frac{\partial G^{(1)}(p_i, q_j)}{\partial N} dl \quad (i, j = 1, \dots, N_I + N_C), \quad (65)$$

and that in the right hand side or $G^{(1)}$ is given as

$$(G^{(1)})_{ij} = \int_{\Delta_j} G^{(1)}(p_i, q_j) dl \quad (i = 1, \dots, N_I + N_C, \quad j = N_I + 1, \dots, N_I + N_C) \quad (66)$$

and

$$\tilde{G}^{(1)}|_{ij} = \frac{L\kappa_m \tanh(\kappa_m H)}{\rho_w \omega^2 Q_m} \int_{\Delta_j} G^{(1)}(p_i, q_j) dl \quad (i = 1, \dots, N_I + N_C, \quad j = 1, \dots, N_I). \quad (67)$$

It may be noted that I and C used in Eq. (64) refer to the element on Γ_I and Γ_C , respectively. Invoking Eq. (64), φ_m can be given as

$$\begin{bmatrix} \varphi_m^I \\ \varphi_m^C \end{bmatrix} = \begin{bmatrix} Q_{II}^{(1)} & Q_{IC}^{(1)} \\ Q_{CI}^{(1)} & Q_{CC}^{(1)} \end{bmatrix} \begin{bmatrix} \Upsilon \\ \frac{\partial \varphi_m^C}{\partial N} \end{bmatrix}, \quad (68)$$

where

$$\begin{bmatrix} Q_{II}^{(1)} & Q_{IC}^{(1)} \\ Q_{CI}^{(1)} & Q_{CC}^{(1)} \end{bmatrix} = \begin{bmatrix} \frac{\partial G_{II}^{(1)}}{\partial N} & \frac{\partial G_{IC}^{(1)}}{\partial N} \\ \frac{\partial G_{CI}^{(1)}}{\partial N} & \frac{\partial G_{CC}^{(1)}}{\partial N} \end{bmatrix}^{-1} \begin{bmatrix} \tilde{G}_{II}^{(1)} & G_{IC}^{(1)} \\ \tilde{G}_{CI}^{(1)} & G_{CC}^{(1)} \end{bmatrix}. \quad (69)$$

This gives

$$[\varphi_m^I] = [Q_{II}^{(1)}][\Upsilon] + [Q_{IC}^{(1)}] \left[\frac{\partial \varphi_m^C}{\partial N} \right]. \quad (70)$$

Substituting Eqs. (70) into (19) and invoking the clamped ice edge condition Eq. (10), we have at panel i of Γ_I ,

$$\sum_{m=-2}^{M-3} \varphi_m^I(p_i) \frac{d\psi_m(z)}{dz} = 0 \quad (z = 0, i = 1, 2, \dots, N_I) \quad (71)$$

or

$$\sum_{m=-2}^{M-3} \kappa_m \tanh(\kappa_m H) \left\{ [Q_{II}^{(1)}][\Upsilon] + [Q_{IC}^{(1)}] \left[\frac{\partial \varphi_m^C}{\partial N} \right] \right\} = 0 \quad (i = 1, 2, \dots, N_I). \quad (72)$$

Once $[\Upsilon]$ is solved through (72), Eq. (30) gives on Γ_I ,

$$\frac{\partial \varphi_m^I}{\partial N} = \frac{L\kappa_m \tanh(\kappa_m H)}{\rho_w \omega^2 Q_m} [\Upsilon]. \quad (73)$$

In Ω_2 outside the harbor, Eq. (61) can be discretized as

$$\alpha^{(2)}(p_i)\phi_{\bar{m}}(p_i) = \sum_{j=1}^{N_C} \int_{\Delta_j} \left[G_{\bar{m}}^{(2)}(p_i, q_j) \frac{\partial \phi_{\bar{m}}(q_j)}{\partial N} - \frac{\partial G_{\bar{m}}^{(2)}(p_i, q_j)}{\partial N} \phi_{\bar{m}}(q_j) \right] dl, \quad (i, j = 1, \dots, N_C). \quad (74)$$

While Eqs. (55) and (58) can be discretized and truncated as

$$\varphi_m^C Q_{\bar{m}} = (\varphi_I + \bar{\varphi}_{II}) \mathfrak{S}_{0,\bar{m}} + \sum_{m=0}^{M-1} \phi_m \mathfrak{S}_{m,\bar{m}} + \sum_{m=-2}^{M-3} \mathfrak{R}_{m,\bar{m}} \varphi_m \quad (75)$$

and

$$\frac{\partial \varphi_m^C}{\partial N} Q_{\bar{m}} = \sum_{m=0}^{M-1} \frac{\partial \phi_m}{\partial N} \mathfrak{S}_{m,\bar{m}} + \sum_{m=-2}^{M-3} \mathfrak{R}_{m,\bar{m}} \varphi_m. \quad (76)$$

Equations (63), (72)–(76) provide $2M \times (N_I + 2N_C) + N_I$ equations, the number of which is the same as the unknowns, i.e., φ_m , $\partial \varphi_m / \partial n$, Υ . This means that the overall equations are completed and can be solved simultaneously.

IV. NUMERICAL RESULTS

In following numerical computations, the typical parameters of ice sheet and fluid are taken to be³⁸

$$E = 5 \text{ GPa}, \quad \nu = 0.3, \quad \rho_i = 922.5 \text{ kg m}^{-3}, \quad (77)$$

$$\rho_w = 1025 \text{ kg m}^{-3}, \quad g = 9.80 \text{ m s}^{-2},$$

to provide physical meaningful results. All the results will be presented in the dimensionless form based on the three basic parameters, i.e., density of water ρ_w , acceleration due to gravity g , and a characteristic length scale.

A. Verification of the method and solution procedure

We first consider the wave interactions with a rectangular harbor with its length L_I taken to be the characteristic length scale. The harbor width and depth are set to be $L_w = 0.1943$ and $H = 0.8268$, respectively. The incident wave from the open sea is assumed to propagate normally into the harbor or $\beta = \pi$. The case has been studied by Lee⁴ and Shi, Li, and Wu⁸ when there is no ice sheet on the water surface inside the harbor. As the ice thickness is zero or $L = 0$ and $m = 0$ in Eq. (8), the solution will become that for a free surface harbor. In such

a case, $n = -1, -2$ should be removed from Eq. (19), and Eq. (30) becomes $\partial\varphi_m/\partial N = 0$. While Eqs. (55) and (58) can be simplified as $\varphi_{\bar{m}} = (\varphi_I + \bar{\varphi}_I)\delta_{0,\bar{m}}$ and $\partial\varphi_{\bar{m}}/\partial N = \partial\phi_{\bar{m}}/\partial N$, respectively, which means that in Eqs. (19) and (53), only the terms corresponding to κ_0 and k_0 are nonzero. Figure 2 shows the amplification factor \mathcal{R} at $(-1, 0, 0)$ against the wavenumber k_0 . Here, \mathcal{R} at a given point (x, y) is defined as the ratio of the complex wave amplitude there to that due to $\phi_I + \phi_I^{(2)}$ at the coastal line, or $\zeta = 2\eta \cos(k_0 x \cos \beta) \exp(-ik_0 y \sin \beta)$ which gives $|\zeta| = 2|\eta \cos(k_0 x \cos \beta)|$. Here, the wave amplitude w is determined through kinematic boundary conditions (5), which provides

$$w = \left(\frac{\partial\phi}{\partial z} \right)_{z=0}. \tag{78}$$

As a comparison, the numerical results for $h = 0$ in Shi, Li, and Wu⁸ are also provided. It can be seen from the figure that convergence has been achieved when $N_I = 134$ and $N_C = 12$, and the converged results agree well with those in Shi *et al.*⁸ Computations are then carried out for the rectangular harbor covered by an ice sheet but with very small thickness, i.e., $h = 1 \times 10^{-4}$ and $h = 1 \times 10^{-5}$, while the other parameters are the same as those in Fig. 2. For nonzero h , the infinite series are truncated at $M = 20$ which is found to provide graphically convergent results. When the ice thickness is very small, the solution becomes very close to that for a free surface harbor. This can be observed in Fig. 3, which shows $|\mathcal{R}|$ at $(-0.5, 0, 0)$ against the wave number k_0 with different h .

B. Wave motions in a frozen harbor

We now consider the wave motion in a frozen harbor to show the effect of ice sheet. The shape of the harbor is a combination of a rectangle and a semicircle, as shown in Fig. 4. The length L_I of the rectangle shown in the figure is chosen as the characteristic length scale. The width of the harbor L_w which equals the diameter of the semicircle is set to be $L_w = 0.5$ or $a = 0.25$, and the water depth is chosen as $H = 0.25$. In the following numerical computations, the harbor line Γ_I and interface line Γ_C are, respectively, discretized into $N_I = 279$ and $N_C = 51$ straight line segments, while the first $M = 20$ terms are kept in the infinite series. These are found to provide graphically convergent results.

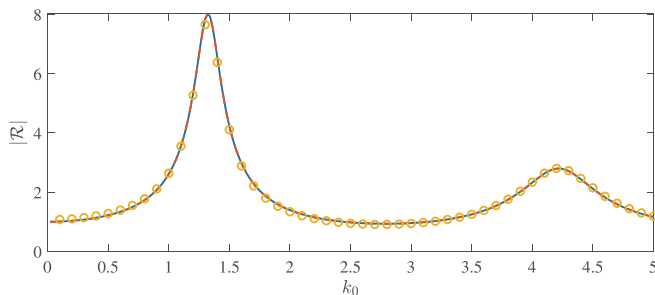


FIG. 2. The modulus of amplification factor \mathcal{R} against k_0 at $(-1, 0, 0)$ of a rectangular harbor. Solid line: $N_I = 134$ and $N_C = 12$; dashed line: $N_I = 269$ and $N_C = 24$; open circles: results from Shi, Li, and Wu.⁸ ($h = 0, \beta = \pi$).

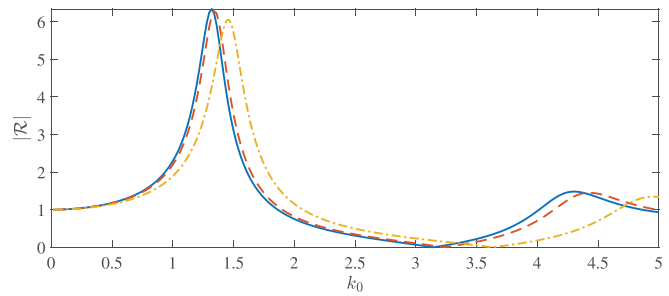


FIG. 3. The modulus of amplification factor \mathcal{R} against k_0 at $(-0.5, 0, 0)$ of a rectangular harbor. Solid line: $h = 0$; dashed line: $h = 1 \times 10^{-5}$; dashed-dotted line: $h = 1 \times 10^{-4}$. ($\beta = \pi, N_I = 134, N_C = 12, M = 20$).

1. The effect of ice thickness on the ice sheet deflection

Figure 5 shows the amplification factor \mathcal{R} at three chosen points inside the harbor against the wavenumber k_0 , namely, $P_1(-1.0, 0, 0)$, $P_2(-0.5, 0, 0)$ and $P_3(0^-, 0, 0)$, together with the point $P_4(0^+, 0, 0)$ outside the harbor. Here, 0^- and 0^+ indicate that the point is approached from the left- and right-hand side, respectively. The incident wave is assumed to propagate normally into the harbor with $\beta = \pi$. Three different ice thicknesses are considered, i.e., $h = 5 \times 10^{-4}, 5 \times 10^{-3}$ and 1×10^{-2} . The results for a free surface harbor with $h = 0$ are also provided. The wavenumber varies from 0.05 to 20 with step $\Delta k_0 = 0.05$ in the calculation. It can be seen from the comparison of results in Figs. 5(c) and 5(d) that $|\mathcal{R}|$ on both sides of the ice edge are different, or the free surface elevation and the ice sheet deflection at the interface line are generally not the same. This is because that although they share the same kinematic boundary condition, the dynamic boundary conditions are different.

As $k_0 \rightarrow 0$, it can be seen that $|\mathcal{R}|$ at $P_4(0^+, 0, 0)$ tends to 1 at different h . This is because that when $k_0 \rightarrow 0, \phi_D^{(2)}$ in Eq. (32) satisfies $\partial\phi_D^{(2)}/\partial z = 0$ on $z = 0$ according to Eq. (15). Therefore, $\phi_D^{(2)}$ does not make an additional contribution to the free surface elevation which is calculated through Eq. (78), while from Eqs. (33)–(35), we have $|\partial(\phi_I + \phi_I^{(2)})/\partial z| = 2$ on $z = 0$. However, this is different on the ice sheet inside the harbor. Equation (22) shows that at $\omega = 0, \kappa_{-2} = -(\rho_w g/L)^{1/4} \exp(i\pi/4), \kappa_{-1} = -(\rho_w g/L)^{1/4} \exp(i3\pi/4)$, and $\kappa_m = -im\pi/H, m = 0, 1, \dots, \infty$. This means that when the operator $\partial/\partial z$ is applied to Eq. (19), the first two terms are not

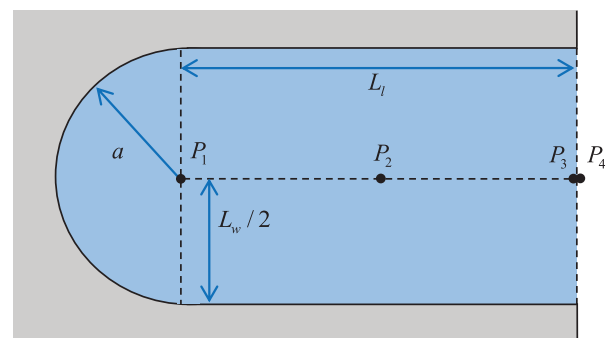


FIG. 4. Plane view of a frozen harbor.

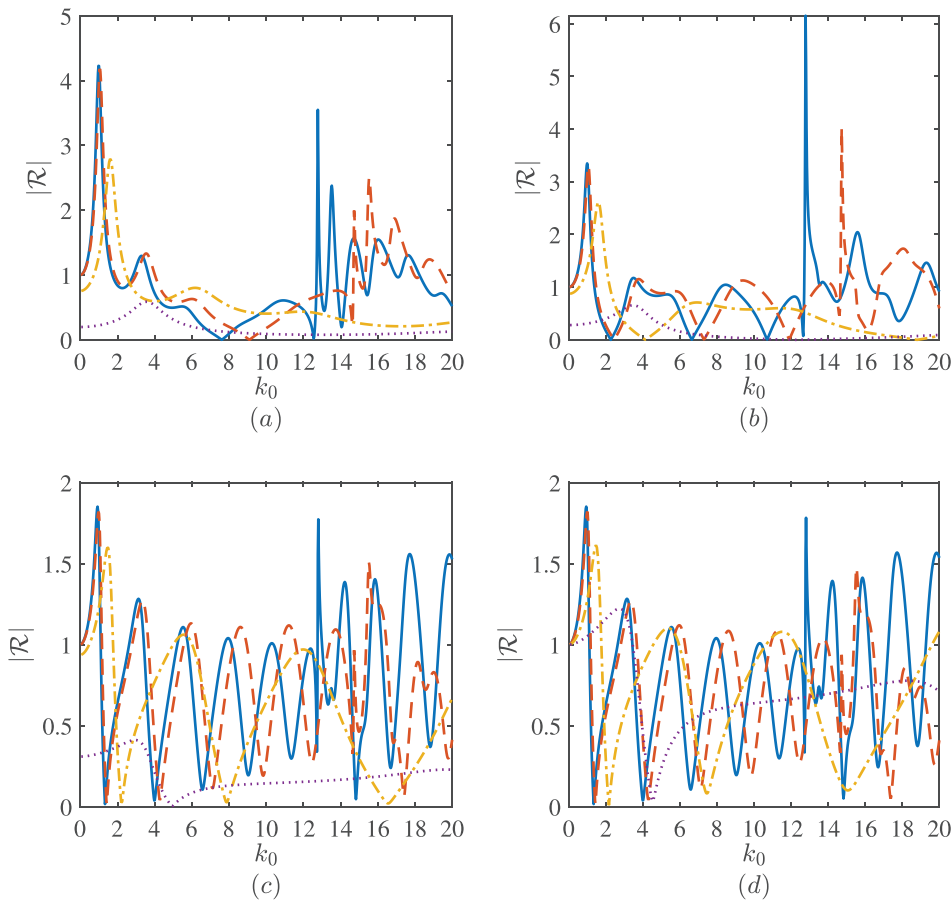


FIG. 5. The modulus of amplification factor \mathcal{R} against k_0 inside the frozen harbor with different ice thickness h . Solid line: $h = 0$; dashed line: $h = 5 \times 10^{-4}$; dashed-dotted line: $h = 5 \times 10^{-3}$; dotted line: $h = 1 \times 10^{-2}$. (a) $P_1(-1.0, 0, 0)$; (b) $P_2(-0.5, 0, 0)$; (c) $P_3(0^-, 0, 0)$; (d) $P_4(0^+, 0, 0)$. ($\beta = \pi$, $N_I = 279$, $N_C = 51$, $M = 20$).

automatically equal to zero on $z = 0$, while those of $m \geq 0$ are. As a result, $\partial\phi^{(1)}/\partial z$ is not automatically zero on $z = 0$ when $k_0 \rightarrow 0$ or $\omega \rightarrow 0$, or \mathcal{R} is nonzero. Also, $\phi^{(1)}$ is not equal to $\phi_I + \phi_I^{(2)}$. Thus, $|\mathcal{R}|$ is not equal to 1 either and its value changes from location to location. When $h = 0$, to match the conditions in Eqs. (38) and (39) more conveniently, we can write $\phi^{(1)} = \phi_I + \phi_I^{(2)} + \phi_D^{(1)}$. Here, $\partial\phi_D^{(1)}/\partial z = 0$ on $z = 0$ as $k_0 \rightarrow 0$. Thus, $|\mathcal{R}|$ is equal to 1 everywhere.

When k_0 increases from zero, $|\mathcal{R}|$ increases very rapidly, especially when ice thickness is small. The first peak of the amplification factor can be larger than 4, deep inside the harbor at $x = -1.0$. As x moves toward the harbor entrance, the first peak of $|\mathcal{R}|$ decreases in the four cases calculated. The results of small ice thickness resemble more closely to those of the full free surface problem. However, even at $h = 5 \times 10^{-4}$, the results are still quite different from those at $h = 0$. Shi, Li, and Wu⁸ gave detailed discussions on the reasons for highly oscillatory behavior of the results at $h = 0$. Similar reasons can be applied here. Figure 6 depicts flexural gravity wavenumber κ_0 against free surface wavenumber k_0 at three different ice thicknesses together with the result for $h = 0$. It can be observed from the figure that as k_0 increases, κ_0 for different ice thicknesses departs from each other. Generally, κ_0 is smaller for a thicker ice sheet at a given k_0 , indicating a larger wavelength. At $h = 5 \times 10^{-4}$, κ_0 is very close to k_0 or

the result at $h = 0$. However, because of the effects of other κ_m , their results in Fig. 5 are not close.

Figure 7 shows the magnitude of the amplification factor \mathcal{R} along the longitudinal cut at $y = 0$ with three different ice thicknesses h together with the results without ice sheet. Two wave numbers are considered, i.e., $k_0 = 10$ and 20 . From the figure, it can be observed that when k_0 is fixed, $|\mathcal{R}|$ is less oscillatory with x at larger h . This is

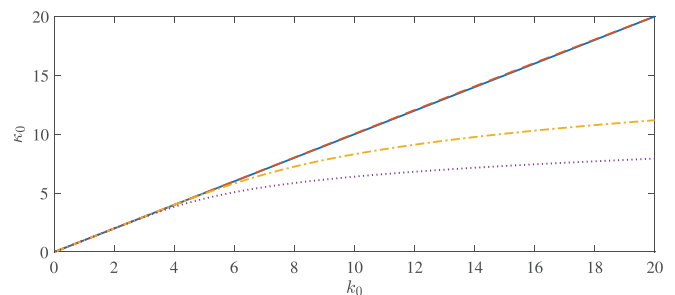


FIG. 6. Flexural gravity wavenumber κ_0 against the free surface wavenumber k_0 at different ice thicknesses h . Solid line: $h = 0$; dashed line: $h = 5 \times 10^{-4}$; dashed-dotted line: $h = 5 \times 10^{-3}$; dotted line: $h = 1 \times 10^{-2}$.

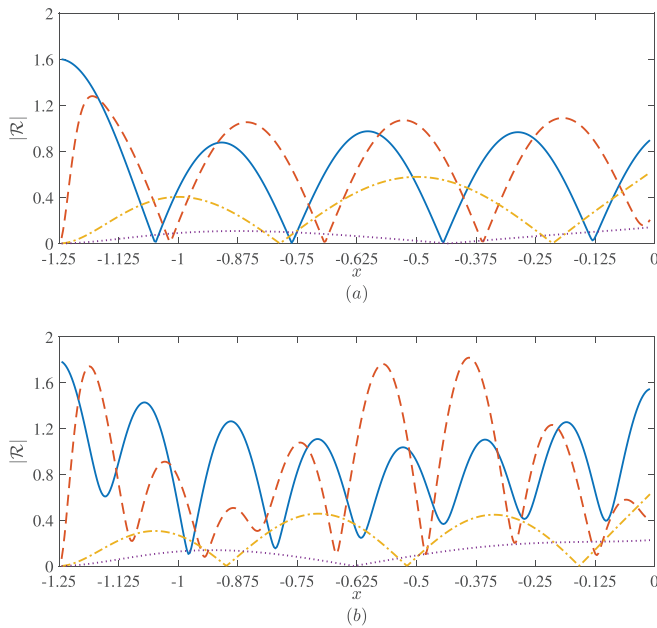


FIG. 7. The modulus of amplification factor \mathcal{R} against x inside the frozen harbor at $y = 0$. Solid line: $h = 0$; dashed line: $h = 5 \times 10^{-4}$; dashed-dotted line: $h = 5 \times 10^{-3}$; dotted line: $h = 1 \times 10^{-2}$. (a) $k_0 = 10$; (b) $k_0 = 20$. ($\beta = \pi$, $N_I = 279$, $N_C = 51$, $M = 20$).

because κ_0 is smaller at larger h , as shown in Fig. 6. It is interesting to see that when h is very small, $|\mathcal{R}|$ is not always smaller than that at $h = 0$. At larger h , the ice sheet becomes more rigid and $|\mathcal{R}|$ becomes smaller overall. It can be also seen from Fig. 7 that for some k_0 and h , there are several points of x at which \mathcal{R} is very small. Figure 8 depicts the contour of $|\mathcal{R}|$ as a function of x and y with the wavenumber taken to be $k_0 = 10$. The ice thickness is chosen as $h = 5 \times 10^{-3}$. As a comparison, $h = 0$ for a free surface harbor is also provided. From the figure, we can observe that for $h = 0$, $|\mathcal{R}|$ does not change that significantly with y in the rectangular section. When there is an ice sheet, or $h \neq 0$, variation of $|\mathcal{R}|$ with y becomes very obvious. As the edge of the ice sheet is clamped to the harbor wall, $\mathcal{R} = 0$ along the edge, as can be seen in Figs. 7 and 8.

2. The effect of incident wave angle on the ice sheet deflection

We now consider the effect of incident wave angle on wave motions inside the harbor. Figure 9 provides the amplification factor \mathcal{R} against the wave number k_0 with different incident wave angles. The ice thickness is taken to be $h = 5 \times 10^{-3}$, and the step and range of k_0 as well as the positions where \mathcal{R} is computed are the same as those in Fig. 5. Four incident wave angles are considered, namely, $\beta = \pi$, $5\pi/6$, $2\pi/3$ and $11\pi/18$, in last of which the incident wave propagates nearly parallel to the coastal line. It can be seen from Eqs. (38) and (39) together with Eq. (32), the driving force for the wave motion inside the harbor is the incident wave and its reflection by the coastal wall. Noticing Eq. (35) and the fact that the matching conditions in Eqs. (38) and (39) are imposed at $x = 0$, the driving term is in

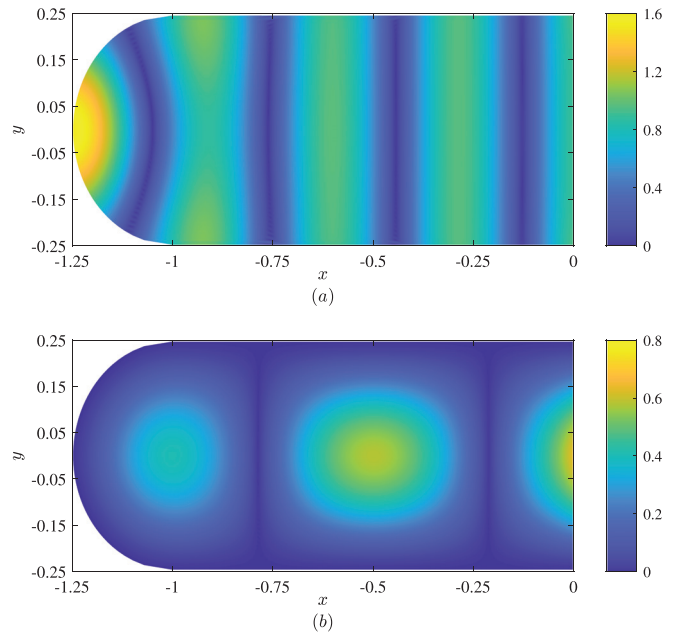


FIG. 8. Contour of the modulus of amplification factor \mathcal{R} . (a) $h = 0$; (b) $h = 5 \times 10^{-3}$. ($\beta = \pi$, $k_0 = 10$, $N_I = 279$, $N_C = 51$, $M = 20$).

the form of $\exp(-ik_0y \sin \beta)$. Therefore, when k_0y is small, the effect of β to the solution is small, and when $k_0 = 0$, the result is independent to β . This can be clearly seen in Fig. 9. Generally, at $P_1(-1.0, 0, 0)$ and $P_2(-0.5, 0, 0)$, or points away from the entrance, $|\mathcal{R}|$ is smaller when β is smaller. This means when the wave is more parallel to the coastal wall, the fluid deep inside the harbor will be less disturbed. This is almost the same near the entrance, or at $P_3(0^-, 0, 0)$. Point $P_4(0^+, 0, 0)$ is on the free surface outside the harbor. At larger k_0 , $|\mathcal{R}|$ can sometimes be larger at smaller β .

Figure 10 depicts the amplification factor \mathcal{R} along the longitudinal cut at $y = 0$ with different incident wave angles β . The wavenumber and ice sheet thickness are taken to be $k_0 = 20$ and $h = 5 \times 10^{-3}$, respectively. The results for a free surface harbor are also provided as a comparison. When other parameters are fixed, different wave direction in fact gives a driving term of different magnitude in Eqs. (38) and (39). It is therefore expected that $|\mathcal{R}|$ will have a similar pattern but different magnitude. This in fact can be observed from Fig. 10. For both the free surface harbor and the frozen harbor, $|\mathcal{R}|$ at different β all oscillates with x in a similar manner. Deep inside the harbor with $h = 0$, $|\mathcal{R}|$ decreases with β . However, this is not the case near the harbor entrance. While for a frozen harbor, \mathcal{R} tends to be zero close to the left end of the harbor for all β due to the clamped ice edge condition, and everywhere else on x , $|\mathcal{R}|$ decreases with β . To show the spatial variations of \mathcal{R} more clearly, in Figs. 11 and 12 the contour of $|\mathcal{R}|$ is provided for $h = 0$ and $h = 5 \times 10^{-3}$, respectively. In both figures, two values of β are considered, i.e., $\beta = \pi$ and $\beta = 11\pi/18$. For the normal incident wave case, the wave elevation inside the harbor is symmetric with respect to x -axis, as expected. When the incident wave becomes nearly parallel to the coastal line, the color of the largest value of $|\mathcal{R}|$ at $h = 0$ is similar to that in the normal incident wave case.

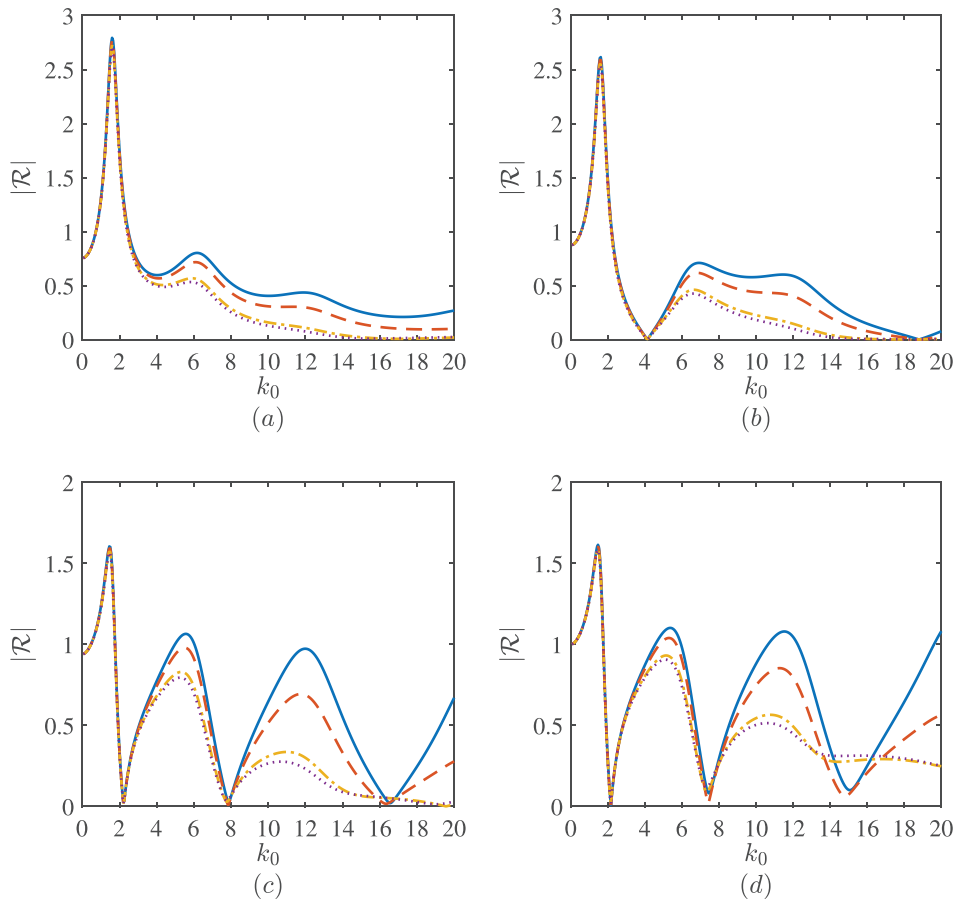


FIG. 9. The modulus of amplification factor \mathcal{R} against k_0 inside the frozen harbor with different incident wave angles β . Solid line: $\beta = \pi$; dashed line: $\beta = 5\pi/6$; dashed-dotted line: $\beta = 2\pi/3$; dotted line: $\beta = 11\pi/18$. (a) $P_1(-1.0, 0, 0)$; (b) $P_2(-0.5, 0, 0)$; (c) $P_3(0^-, 0, 0)$; (d) $P_4(0^+, 0, 0)$. ($h = 5 \times 10^{-3}$, $N_I = 279$, $N_C = 51$, $M = 20$).

However, when the harbor is frozen, \mathcal{R} for $\beta = 11\pi/18$ is almost zero inside the harbor, as has been observed in Figs. 9 and 10. For a frozen harbor, the waves inside and outside the harbor will propagate with different wavenumbers, and at a given wave frequency the wavenumber for the former is generally smaller than the later, as shown in Fig. 6. Specifically, at $k_0 = 20$ and $h = 5 \times 10^{-3}$, we have $\kappa_0/k_0 = 0.5592$. For free surface wave interactions with a semi-infinite ice sheet, or the harbor width L_w being taken as infinity, at the ice edge along $x = 0$, we should have $k_0 \sin(\pi - \beta) = \kappa_0 \sin \alpha^{12}$ with $\beta \in [\pi/2, \pi]$ and $\alpha \in [0, \pi/2]$, where α is the angle between transmitted progressing wave and ice edge. When $\alpha = \pi/2$, β corresponds to a critical angle, i.e., $\beta_c = \pi - \arcsin(\kappa_0/k_0)$. When β is smaller than β_c there will be no wave transmitted into the ice sheet. For $\kappa_0/k_0 = 0.5592$, we have $\beta_c = 2.5482$ and $\beta = 11\pi/18 \approx 1.9199 < \beta_c$. In such a case, there will be no wave below the ice sheet when $L_w = \infty$. For a finite L_w , the wave motion may not be exactly zero, but is expected to be small, which is reflected in Fig. 12(b).

V. CONCLUSIONS

The problem of ocean wave interactions with a harbor covered by an ice sheet clamped to the harbor wall has been solved, based on the linearized velocity potential theory and thin elastic plate model. A domain decomposition methodology is developed, which decomposes

the problem into two subdomains, i.e., one inside the harbor and the other outside the harbor. The velocity potential inside the harbor is written in terms of eigenfunction series in the vertical direction satisfying the bottom and ice sheet conditions. Each of the functions in the horizontal plane satisfies the Helmholtz equation which is further transformed into an integral equation along the ice edge. By adopting an orthogonal inner product, the conditions on the harbor wall and ice edge are satisfied. Outside the harbor, the velocity potential is written as an integral equation through the modified free surface Green function, which does not involve the coastline. The pressures and the velocities inside and outside the harbor are matched at the interface by using the orthogonal inner product, through which the ice edge condition at the harbor entrance is also satisfied. Numerical solutions are obtained through the boundary element method.

From the results of a rectangular harbor, it is demonstrated that when the thickness of ice sheet inside the harbor is very small, the result will become close to that for a free surface harbor. The developed method is applicable to a harbor of an arbitrary horizontal geometry. This is demonstrated through a case study using a shape that is composed of a rectangle and semicircle. It is found in the case study that on both sides of the harbor entrance or at the ice edge, the wave elevation is different due to the difference of the dynamic boundary conditions. As the free surface wavenumber $k_0 \rightarrow 0$, the modulus of

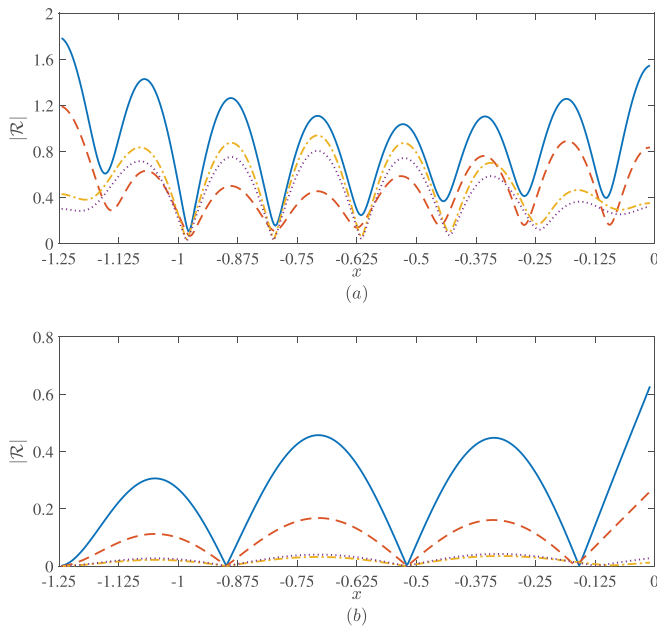


FIG. 10. The modulus of amplification factor \mathcal{R} against x inside the frozen harbor at $y = 0$. Solid line: $\beta = \pi$; dashed line: $\beta = 5\pi/6$; dashed-dotted line: $\beta = 2\pi/3$; dotted line: $\beta = 11\pi/18$. (a) $h = 0$; (b) $h = 5 \times 10^{-3}$. ($k_0 = 20$, $N_I = 279$, $N_C = 51$, $M = 20$).

amplification factor $|\mathcal{R}|$ inside the harbor with an ice sheet is generally small than 1, while $|\mathcal{R}|$ outside the harbor tends to 1. When ice sheet thickness h is very small, $|\mathcal{R}|$ inside the harbor becomes very close to 1 as $k_0 \rightarrow 0$. When h increases, the flexural gravity wavenumber k_0

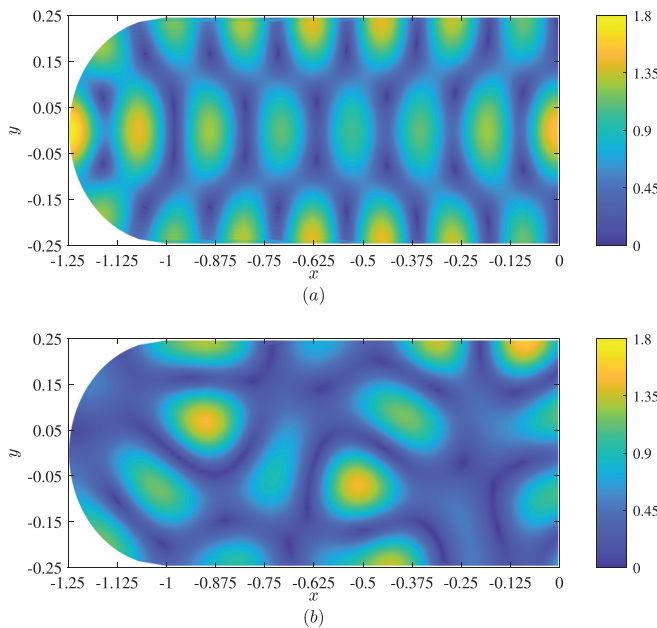


FIG. 11. Contour of the modulus of amplification factor \mathcal{R} . (a) $\beta = \pi$; (b) $\beta = 11\pi/18$. ($h = 0$, $k_0 = 20$, $N_I = 279$, $N_C = 51$, $M = 20$).

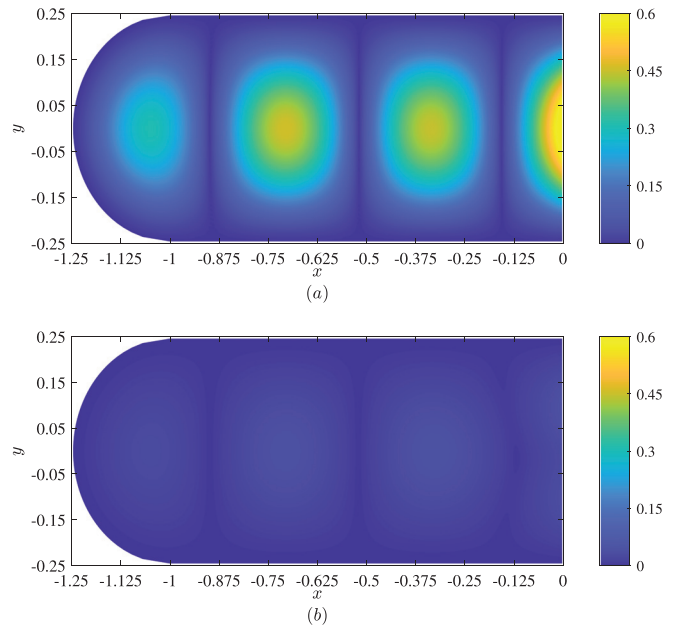


FIG. 12. Contour of the modulus of amplification factor \mathcal{R} . (a) $\beta = \pi$; (b) $\beta = 11\pi/18$. ($h = 5 \times 10^{-3}$, $k_0 = 20$, $N_I = 279$, $N_C = 51$, $M = 20$).

decreases and $|\mathcal{R}|$ is less oscillatory spatially. Overall, $|\mathcal{R}|$ decreases with the increase in h , but when h is very small, $|\mathcal{R}|$ at some places inside the harbor can be larger than that at $h = 0$. As the angle between the incident wave and the coastline becomes smaller, $|\mathcal{R}|$ inside the harbor is generally smaller, but $|\mathcal{R}|$ outside the harbor can sometimes be larger at large k_0 . When the incident wave is nearly parallel to the coastline, $|\mathcal{R}|$ inside a frozen harbor is almost zero everywhere. This is different from a harbor with $h = 0$, at which the largest value of $|\mathcal{R}|$ corresponding to oblique incident wave is similar to that corresponding to the normal incident wave.

ACKNOWLEDGMENTS

This work is supported by Lloyd’s Register Foundation, to which the authors are most grateful. Lloyd’s Register Foundation helps to protect life and property by supporting engineering-related education, public engagement, and the application of research. This work is also supported by the National Natural Science Foundation of China (Grant Nos. 51709131, 52071162, 52025112 and 51879123).

DATA AVAILABILITY

The data that support the findings of this study are available from the corresponding author upon reasonable request.

REFERENCES

- ¹J. S. Mcnown, “Waves and seiche in idealized ports,” in *Proceedings of NBS Semicentennial Symposium on Gravity Waves* (Nat. Bureau Standards Circular, 1952), Vol. 521.
- ²J. Kravtchenko and J. S. Mcnown, “Seiche in rectangular ports,” *Q. Appl. Math.* **13**, 19 (1955).
- ³L. S. Hwang and E. O. Tuck, “On the oscillations of harbours of arbitrary shape,” *J. Fluid Mech.* **42**, 447 (1970).

23 April 2024 12:06:46

- ⁴J. J. Lee, "Wave-induced oscillations in harbours of arbitrary geometry," *J. Fluid Mech.* **45**, 375 (1971).
- ⁵M. Isaacson and S. Q. Qu, "Waves in a harbour with partially reflecting boundaries," *Coastal Eng.* **14**, 193 (1990).
- ⁶K. I. Hamanaka, "Open, partial reflection and incident-absorbing boundary conditions in wave analysis with a boundary integral method," *Coastal Eng.* **30**, 281 (1997).
- ⁷P. Kumar, H. Zhang, K. I. Kim, Y. L. Shi, and D. A. Yuen, "Wave spectral modeling of multidirectional random waves in a harbor through combination of boundary integral of Helmholtz equation with Chebyshev point discretization," *Comput. Fluids* **108**, 13 (2015).
- ⁸Y. Y. Shi, Z. F. Li, and G. X. Wu, "Motion of a floating body in a harbour by domain decomposition method," *Appl. Ocean Res.* **78**, 223 (2018).
- ⁹V. A. Squire, "Of ocean waves and sea-ice revisited," *Cold Reg. Sci. Technol.* **49**, 110 (2007).
- ¹⁰V. A. Squire, "Ocean Wave Interactions with Sea Ice: A Reappraisal," *Annu. Rev. Fluid Mech.* **52**, 37 (2020).
- ¹¹C. Fox and V. A. Squire, "Reflection and transmission characteristics at the edge of shore fast sea ice," *J. Geophys. Res. Oceans* **95**, 11629, <https://doi.org/10.1029/JC095iC07p11629> (1990).
- ¹²C. Fox and V. A. Squire, "On the oblique reflexion and transmission of ocean waves at shore fast sea ice," *Philos. Trans. R. Soc., A* **347**, 185 (1994).
- ¹³T. Sahoo, T. L. Yip, and A. T. Chwang, "Scattering of surface waves by a semi-infinite floating elastic plate," *Phys. Fluids* **13**, 3215 (2001).
- ¹⁴D. V. Evans and T. V. Davies, "Wave-ice interaction," Document Number 1313, 1968.
- ¹⁵N. J. Balmforth and R. V. Craster, "Ocean waves and ice sheets," *J. Fluid Mech.* **395**, 89 (1999).
- ¹⁶H. Chung and C. Fox, "Calculation of wave-ice interaction using the Wiener-Hopf technique," *New Zealand J. Math.* **31**, 1 (2002).
- ¹⁷L. A. Tkacheva, "The diffraction of surface waves by a floating elastic plate at oblique incidence," *J. Appl. Math. Mech.* **68**, 425 (2004).
- ¹⁸C. M. Linton and H. Chung, "Reflection and transmission at the ocean/sea-ice boundary," *Wave Motion* **38**, 43 (2003).
- ¹⁹M. Meylan and V. A. Squire, "Finite-floe wave reflection and transmission coefficients from a semi-infinite model," *J. Geophys. Res. Oceans* **98**, 12537, <https://doi.org/10.1029/93JC00940> (1993).
- ²⁰M. Meylan and V. A. Squire, "The response of ice floes to ocean waves," *J. Geophys. Res. Oceans* **99**, 891, <https://doi.org/10.1029/93JC02695> (1994).
- ²¹M. Meylan and V. A. Squire, "Response of a circular ice floe to ocean waves," *J. Geophys. Res.: Oceans* **101**, 8869, <https://doi.org/10.1029/95JC03706> (1996).
- ²²C. D. Wang and M. Meylan, "A higher-order-coupled boundary element and finite element method for the wave forcing of a floating elastic plate," *J. Fluids Struct.* **19**, 557 (2004).
- ²³Y. Y. Shi, Z. F. Li, and G. X. Wu, "Interaction of wave with multiple wide polynyas," *Phys. Fluids* **31**, 067111 (2019).
- ²⁴Z. F. Li, G. X. Wu, and C. Y. Ji, "Wave radiation and diffraction by a circular cylinder submerged below an ice sheet with a crack," *J. Fluid Mech.* **845**, 682 (2018).
- ²⁵Z. F. Li, G. X. Wu, and Y. Y. Shi, "Wave diffraction by a circular crack in an ice sheet floating on water of finite depth," *Phys. Fluids* **30**, 117103 (2018).
- ²⁶Z. F. Li, G. X. Wu, and K. Ren, "Wave diffraction by multiple arbitrary shaped cracks in an infinitely extended ice sheet of finite water depth," *J. Fluid Mech.* **893**, A14 (2020).
- ²⁷P. Brocklehurst, A. A. Korobkin, and E. I. Părău, "Interaction of hydro-elastic waves with a vertical wall," *J. Eng. Math.* **68**, 215 (2010).
- ²⁸J. Bhattacharjee and C. G. Soares, "Flexural gravity wave over a floating ice sheet near a vertical wall," *J. Eng. Math.* **75**, 29 (2012).
- ²⁹P. Brocklehurst, A. A. Korobkin, and E. I. Părău, "Hydroelastic wave diffraction by a vertical cylinder," *Philos. Trans. R. Soc.* **369**, 2832 (2011).
- ³⁰A. A. Korobkin, S. Malenica, and T. Khabakpasheva, "Interaction of flexural-gravity waves in ice cover with vertical walls," *Philos. Trans. R. Soc.* **376**, 20170347 (2018).
- ³¹K. Ren, G. X. Wu, and C. Y. Ji, "Diffraction of hydroelastic waves by multiple vertical circular cylinders," *J. Eng. Math.* **113**, 45 (2018).
- ³²V. A. Squire, "Past, present and impending hydroelastic challenges in the polar and subpolar seas," *Philos. Trans. R. Soc.* **369**, 2813 (2011).
- ³³S. P. Timoshenko and K. S. Woinowsky, *Theory of Plates and Shells* (McGraw-Hill, Singapore, 1959).
- ³⁴Z. F. Li, Y. Y. Shi, and G. X. Wu, "A hybrid method for linearized wave radiation and diffraction problem by a three dimensional floating structure in a polynya," *J. Comput. Phys.* **412**, 109445 (2020).
- ³⁵D. G. Duffy, *Green's Functions with Applications* (CRC Press, New York, 2015).
- ³⁶M. Abramowitz and I. A. Stegun, *Handbook of Mathematical Functions* (Dover Press, New York, 1965).
- ³⁷J. V. Wehausen and E. V. Laitone, *Surface Waves* (Springer Verlag, Berlin, 1960).
- ³⁸V. A. Squire, J. P. Dugan, P. Wadhams, P. J. Rottier, and A. K. Liu, "Of ocean waves and sea ice," *Annu. Rev. Fluid Mech.* **27**, 115 (1995).